Self-assembly of the toll-like receptor agonist macrophage-activating lipopeptide MALP-2 and of its constituent peptide

Article

pubs.acs.org/Biomac

Self-Assembly of the Toll-Like Receptor Agonist Macrophage-Activating Lipopeptide MALP-2 and of Its Constituent Peptide

Valeria Castelletto,[†] Steven Kirkham,[†] Ian W. Hamley,*[,†] Radoslaw Kowalczyk,[†] Martin Rabe,[‡] Mehedi Reza,[§] and Janne Ruokolainen[§]

[†]School of Chemistry, Pharmacy and Food Biosciences, University of Reading, Whiteknights, Reading, RG6 6AD, United Kingdom

[‡]Max-Planck-Institut für Eisenforschung, Max-Planck-Straße 1D, 40237 Düsseldorf, Germany

[§]Department of Applied Physics, Aalto University School of Science, P.O. Box 15100, FI-00076 Aalto, Finland

Supporting Information

ABSTRACT: The self-assembly of the macrophage-activating lipopeptide MALP-2 in aqueous solution has been investigated and is compared to that of the constituent peptide GNNDESNISFKEK. MALP-2 is a toll-like receptor agonist lipopeptide with diverse potential biomedical applications and its self-assembly has not previously been examined. It is found to self-assemble, above a critical aggregation concentration (*cac*), into remarkable "fibre raft" structures, based on lateral aggregation of *β*-sheet based bilayer tapes. Peptide GNNDESNISFKEK also forms *β*-sheet structures above a *cac*, although the morphology is distinct, comprising highly extended and twisted tape structures. A detailed insight into the molecular packing within the MALP-2 raft and GNNDESNISFKEK nanotape structures is obtained through X-ray diffraction and small-angle X-ray scattering. These results point to the significant influence of the attached lipid chains on the self-assembly motif, which lead to the raft structure for the lipopeptide assemblies.

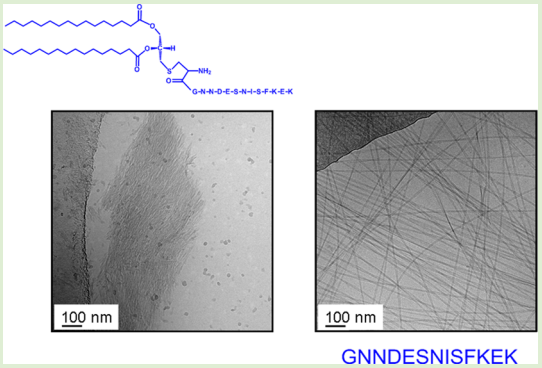

INTRODUCTION

The lipopeptide MALP-2, where MALP stands for macrophage-activating lipopeptide and 2 indicates 2 kDa, is a toll-like receptor (TLR) agonist. MALP-2 comprises a 13-residue peptide GNNDESNISFKEK attached to a (2*R*)-3-((2-amino-3-oxobutyl)thio)propane-1,2-diyl dipalmitate lipid chain (Scheme 1).[1] TLRs are transmembrane proteins with a key role in the immune system and as such are important therapeutic targets.[2] They are activated by Gram -negative bacterial lipopolysaccharides (LPSs), which are so-called endotoxins. Addition of lipid chains to peptides significantly influences their amphiphilicity, leading to potential self-assembly. For TLR agonist lipopeptides, self-assembly and its relationship to bioactivity has hardly been examined to date. In one study it was reported that lipid A (the lipid part of LPS from *E. coli*) forms small aggregates and that these show bioactivity (tumor necrosis factor TNF*α* production cell assays), whereas monomer does not.[3] Earlier reports provided conflicting results. Whereas Shnyra et al. reported that aggregated LPS shows enhanced endotoxic activity compared to a less aggregated form,[4] Takayama et al. found enhanced stimulating activity of LPS in a disaggregated monomeric state.[5] The present study builds on our recent work examining the self-assembly of TLRs,[6] with the ultimate aim to investigate whether there is any relationship between self-assembly and bioactivity for these compounds. MALP-2 was originally isolated from *Mycoplasma fermentas*,[1,7] although synthetic versions are now available commercially. MALP-2 has potential pharmaceutical applications, including use in cancer treatment,[8] wound healing,[9] treatment of sepsis,[10] as a vaccine adjuvant,[10] or in the treatment of pneumonia.[11]

Lipopeptides, also known as peptide amphiphiles (PAs), are a class of biomolecules capable of undergoing self-assembly, driven in part by hydrophobic interactions associated with the lipid chains and in part by interactions among the peptide headgroups, including electrostatic interactions, aromatic stacking interactions, and hydrogen bonding. The latter can lead to ordered secondary structures such as *β*-sheets, which are commonly observed for extended fibrillar self-assemblies.[12] There has been much progress recently in the development of designed PAs incorporating one or more lipid chains (typically palmitoyl) attached to a variety of bioactive peptides. The attachment of lipid chains leads to aggregation, typically into fibrils, upon the surface of which the active peptide motif is presented at high density, often leading to enhanced bioactivity compared to the peptide itself.[12] The excitement resulting from the potential use of these systems in biomedical applications has stimulated us to investigate several lipopeptides already

Received: November 23, 2015
Revised: January 5, 2016
Published: January 10, 2016

DOI: 10.1021/acs.biomac.5b01573
Biomacromolecules 2016, 17, 631−640

Scheme 1. Molecular Structure of MALP-2

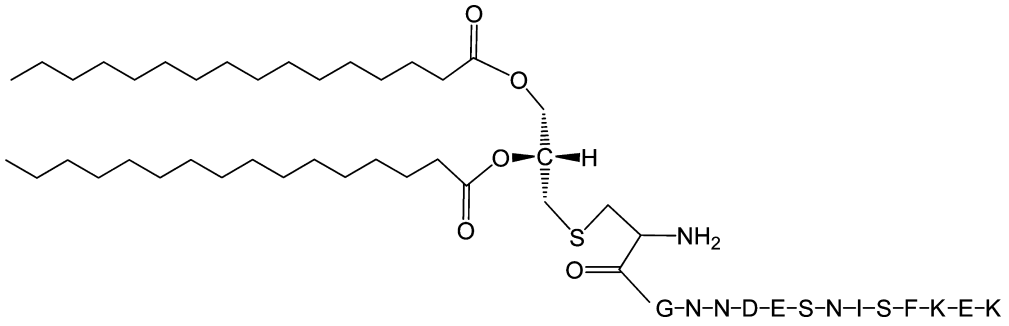

commercially available due to their toll-like receptor activity, focusing on the so-far unstudied self-assembly properties. This work forms part of this ongoing activity.

As part of this program to investigate the self-assembly of bioactive lipopeptides,[13] we recently studied the self-assembly of a related series of three TLR agonist lipopeptides $PAMCSK_4$, PAM_2CSK_4, and PAM_3CSK_4, each containing the CSK_4 peptide headgroup along with one, two, or three C_{16} (palmitoyl, PAM) lipid chains.[6] $PAMCSK_4$ and PAM_2CSK_4 were shown to self-assemble into spherical micelles with an unordered peptide conformation, whereas, in contrast, PAM_3CSK_4 forms wormlike structures based bilayers with peptides adopting β-sheet structures.[6]

Here we develop this research by examining for the first time the self-assembly of the TLR agonist lipopeptide MALP-2. This lipopeptide has the structure *S*-(2,3-*bis*-palmitoyl-(2*R*)-oxypropyl)cysteine-GNNDESNISFKEK (Scheme 1; the extract from *Mycoplasma fermentans* contained C_{18} as well as C_{16} lipid chains[1]). MALP-2 signals via TLR2/TLR6 heterodimers with the cell surface cluster of differentiation protein CD36 as coreceptor.[7,14] In contrast, PAM_3CSK_4 acts on TLR1/2 heterodimers. A summary of the TLR recognition of microbial components is available.[15] MALP-2 is potent in stimulating macrophages or monocytes at pM concentrations.[16]

To the best of our knowledge, the self-assembly of MALP-2 has not previously been investigated. We also study the self-assembly of the peptide component of MALP-2, that is, the 13-residue peptide GNNDESNISFKEK, to evaluate the influence of peptide versus lipid chain units in the self-assembly process. We apply a combination of spectroscopic, microscopic, and X-ray scattering methods to elucidate the secondary structure and mode of assembly of MALP-2 and its constituent peptide.

EXPERIMENTAL SECTION

Materials. MALP-2 (Scheme 1) was custom synthesized by Peptide Synthetics (U.K.). The average molecular mass was 2137.2 g mol^{-1} (expected 2135.2 g mol^{-1}) with a purity >95%, as determined from analytical HPLC. The synthesis of this material is described in detail elsewhere,[17] although Peptide Synthetics have followed prior literature reports[18] to synthesize the lipid chain to which the peptide has been added by conventional stepwise solid phase peptide synthesis techniques. The starting material is an epoxide, (*S*)-(−)glycidol (Sigma-Aldrich). NMR data for the (2*R*)-3-((2-amino-3-oxobutyl)-thio)propane-1,2-diyl dipalmitate lipid chain are provided in the Supporting Information.

Samples were dissolved in water. All data are presented for samples at 0.5 wt % MALP-2 in water unless stated.

GNNDESNISFKEK, the peptide sequence in MALP-2 (Scheme 1), was custom synthesized by Peptide Synthetics (U.K.). The average molecular mass was 1481.520 g mol^{-1} (expected 1481.54 g mol^{-1}) with purity >95%, as determined from analytical HPLC.

Fluorescence Spectroscopy. ANS (8-anilo-1-naphthalenesulfonic acid) and Thioflavin T (ThT) fluorescence were used to locate the critical aggregation concentration (*cac*). Spectra were recorded with a Varian Cary Eclipse fluorescence spectrometer with samples in 4 mm inner width quartz cuvettes. The ANS fluorophore is a probe sensitive to the hydrophobicity of its surrounding environment,[19] making it suitable to determine the *cac*. ANS assays were performed measuring spectra from 400 to 670 nm (λ_{ex} = 356 nm), using a 74 μM ANS solution to solubilize the peptide. ThT fluorescence depends on the formation of amyloid-like structures[20] (β-sheet fibrils) and is used for amyloid fibril-forming peptides. For the ThT assay, the spectra were recorded from 460 to 600 nm using an excitation wavelength λ_{ex} = 440 nm, and the peptide was dissolved in a 5.0×10^{-3} wt % ThT solution.

Fourier Transform Infra-Red (FTIR) Spectroscopy. Variable temperature FTIR experiments for MALP-2 and GNNDESNISFKEK were performed using a PerkinElmer Spectrum II FTIR spectrometer. Solutions in D_2O were sandwiched between two CaF_2 plate windows, with a 0.0533 mm thick Teflon spacer. The plate sandwich was heated and cooled using a Specac 4000 series high stability heating controller, and a Specac electrical heating jacket. Experiments were performed by increasing the temperature from 25 to 60 °C with a 5 °C step at a rate ~1 °C/min. The temperature was then reduced to 25 °C at a rate ~2 °C/3 min.

A D_2O background spectrum was subtracted from the spectrum of each sample. For temperature dependent FTIR, the D_2O spectra was measured as a function of the temperature and subtracted from the FTIR of the sample at the corresponding temperature. After D_2O subtraction, a constant baseline of 0.013 and −0.003 was subtracted from the spectra for MALP-2 and GNNDESNISFKEK.

Circular Dichroism. CD spectra were recorded using a Chirascan spectropolarimeter (Applied Photophysics, U.K.). Spectra are presented with absorbance $A < 2$ at any measured point with a 0.5 nm step, 1 nm bandwidth, and 1 s collection time per step. The spectrum from water was subtracted as background.

For MALP-2, CD spectra were measured for increasing temperatures in the range 25−70 °C, using a 10 °C temperature step. The solution was equilibrated at each temperature point for 2 min before measurements were taken. Quartz plaques (0.1 mm thick) were loaded with 0.5 wt % MALP-2 for the CD experiments.

GNNDESNISFKEK solutions were measured using parallel plaques (0.01 mm gap) for concentrations 0.5−2 wt % and a quartz cuvette (1 mm thick) for 0.008 wt %. The CD spectra for 0.008−1 wt % were smoothed using the Chirascan instrument software, confirming that the residual trace shows only noise randomly distributed about zero.

Small-Angle X-ray Scattering (SAXS). SAXS experiments were performed on beamline B21 at Diamond using a BioSAXS robot. Solutions were loaded into the 96-well plate of an EMBL BioSAXS robot and then injected via an automated sample exchanger into a quartz capillary (1.8 mm internal diameter) in the X-ray beam. The quartz capillary was enclosed in a vacuum chamber, in order to avoid parasitic scattering. After the sample was injected in the capillary and reached the X-ray beam, the flow was stopped during the SAXS data acquisition. B21 operated with a fixed camera length (3.9 m) and fixed energy (12.4 keV). The images were captured using a Pilatus 2 M

DOI: 10.1021/acs.biomac.5b01573
Biomacromolecules 2016, 17, 631−640

detector. Data processing (background subtraction, radial averaging) was performed using the dedicated beamline software Scatter.

X-ray Diffraction (XRD). XRD was performed on a peptide stalk prepared by drawing a fiber of a 1 or 10 wt % peptide solution between the ends of wax-coated capillaries. After separation of the capillaries and drying, a stalk was left on the end of one capillary. MALP-2 stalks were mounted (vertically) onto the goniometer of an Oxford Instruments Gemini X-ray diffractometer, equipped with a Sapphire 3 CCD detector. The sample-to-detector distance was 45 mm. GNNDESNISFKEK stalks were mounted vertically onto the four axis goniometer of a RAXIS IV++ X-ray diffractometer (Rigaku) equipped with a rotating anode generator, while the XRD data was collected using a Saturn 992 CCD camera. The sample-to-detector distance was 50 mm. CLEARER software[21] was used to reduce the 2D data to a one-dimensional intensity profile.

Cryogenic Transmission Electron Microscopy (Cryo-TEM). Experiments were carried out using a field emission cryo-electron microscope (JEOL JEM-3200FSC) operating at 300 kV. Images were taken using bright-field mode and zero loss energy filtering (omega type) with a slit width 20 eV. Micrographs were recorded using a Gatan Ultrascan 4000 CCD camera. The specimen temperature was maintained at −187 °C during the imaging. Vitrified specimens were prepared using an automated FEI Vitrobot device using Quantifoil 3.5/1 holey carbon copper grids with 3.5 μm hole sizes. Grids were cleaned using a Gatan Solarus 9500 plasma cleaner just prior to use and then transferred into the environmental chamber of a FEI Vitrobot at room temperature and 100% humidity. Thereafter, 3 μL of sample solution at 0.5 wt % concentration was applied on the grid, blotted once for 1 s, and then vitrified in a 1/1 mixture of liquid ethane and propane at −180 °C. Grids with vitrified sample solutions were maintained in a liquid nitrogen atmosphere and then cryo-transferred into the microscope.

RESULTS AND DISCUSSION

Self-Assembly of MALP-2. The critical aggregation concentration (*cac*) of MALP-2 was obtained from assays using fluorescent dyes. We have performed assays that are sensitive both to the formation of hydrophobic domains (ANS)[19,22] and to the formation of β-sheet "amyloid" structures (Thioflavin T, ThT).[20,23] ANS has been selected as a less toxic alternative to pyrene used in previous measurements of lipopeptide *cac* values by ourselves and others.[24] As shown by the data in Figure 1, the *cac* from the ANS assay is 1.8 × 10^{-3} wt %. The *cac* by Thioflavin T fluorescence is 2.7 × 10^{-3} wt %. This value is in good agreement with that obtained from the ANS fluorescence assay and indicates that β-sheet formation occurs concurrently with the formation of aggregates with sequestered hydrophobic domains. We have previously noted good agreement between *cac* values obtained by hydrophobic dye (pyrene) and ThT fluorescence assays,[25] although this is not necessarily the case a priori since scenarios where hydrophobic collapse occurs independently of β-sheet formation can readily be envisaged and have, in fact, been observed.[26]

We next determined the secondary structure of the peptide motif within MALP-2 using a combination of circular dichroism (CD) and FTIR spectroscopies. The thermal dependence was studied since we have previously noted that the self-assembly of some lipopeptides depends on lipid chain melting events which may occur around 40−50 °C for C_{16} (palmitoyl) lipopeptides[6,13a] or lipids (for example, DPPC[27]). This behavior is not observed for all the lipopeptides we have examined since intermolecular interactions involving the peptide headgroup can influence the ordering of the lipid chains and suppress any lipid chain melting process.

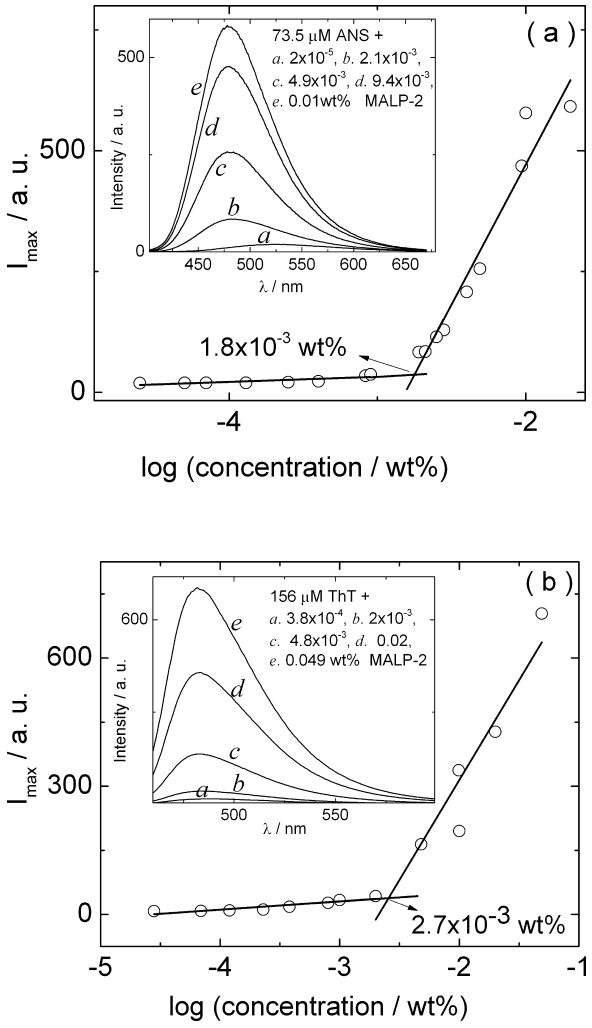

Figure 1. (a) ANS and (b) ThT fluorescence assays to determine the critical aggregation concentration of MALP-2. I_{max} is the intensity at the maximum of the emission curve shown in the inset for some representative concentrations (λ_{ex} = 356 and 440 nm for ANS and ThT, respectively).

FTIR spectra measured as a function of increasing temperature from 25 to 60 °C for a sample containing 0.5 wt % MALP-2, are shown in Figure 2a,b. The spectrum recorded after cooling to 25 °C from 60 °C is also shown. The assignment of a β-sheet secondary structure was confirmed by FTIR in Figure 2a. The presence of a peak at 1622 cm^{-1}, which is independent of temperature over the range studied, is consistent with a β-sheet secondary structure.[28] There is also a sharp peak at 1672 cm^{-1} due to bound TFA counterions[29] (Figure 2a). Figure S2a shows a deconvolution of the background-corrected FTIR spectra in the amide I' region showing the substantial contribution from the 1622 cm^{-1} β-sheet peak, but with additional peaks from the TFA peak and from a peak near 1640 cm^{-1}, which is tentatively assigned to unordered structures.

Figure 2b displays the region of the FTIR spectra corresponding to the CH_2 stretching modes of the lipid chains,[27b] showing bands centered at ∼2850 and ∼2920 cm^{-1}. The temperature dependence of difference spectra (with respect to 25 °C) in the 2900−2950 cm^{-1} range is shown in Figure S2b. There is a clear change in the intensity of the peaks and a small shift in peak position with temperature. However,

DOI: 10.1021/acs.biomac.5b01573
Biomacromolecules 2016, 17, 631−640

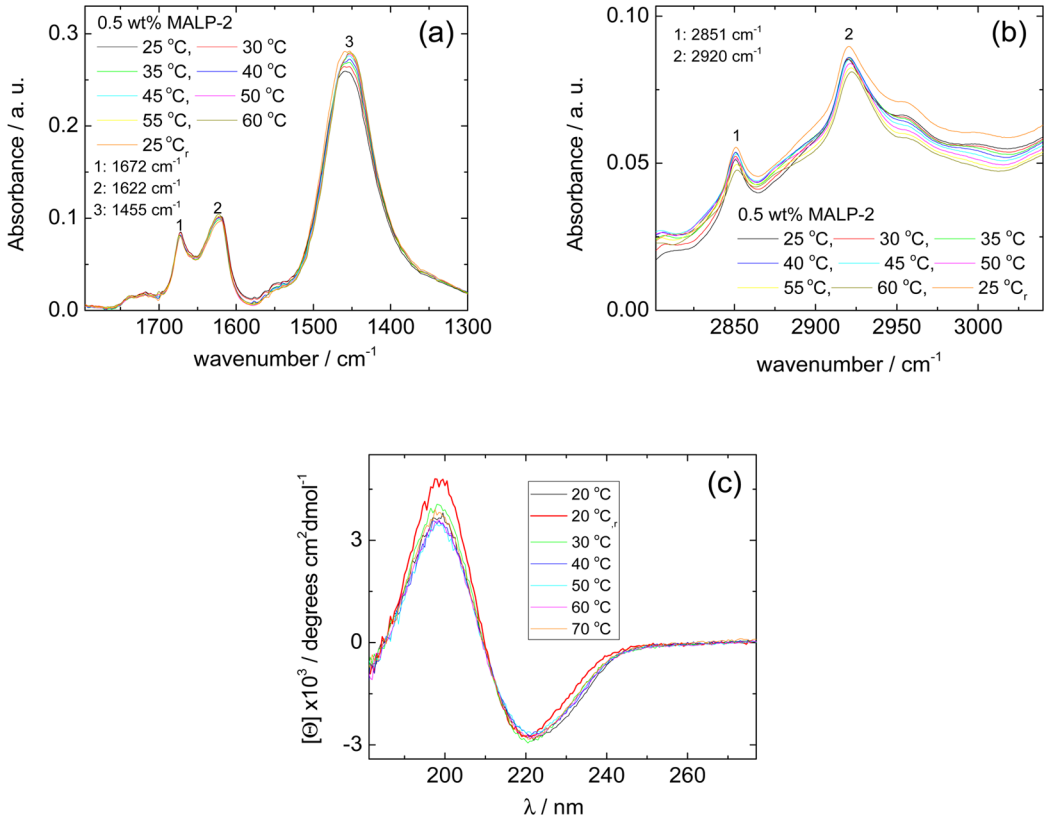

Figure 2. (a, b) FTIR spectra obtained from a 0.5 wt % solution of MALP-2 for a temperature ramp between 25 and 80 °C and at 25 °C on cooling (labeled 25 °C$_r$) in two ranges of wavenumber. (c) Temperature-dependent CD spectra obtained for 0.5 wt % MALP-2.

there was no clear evidence for a sharp lipid chain melting transition in the range 25−60 °C. In the case of lipids, there is a discontinuity across the gel−liquid crystal (L_α) phase transition.[27,30] Such a discontinuity is not observed for MALP-2, rather there is a progressive increase in lipid chain flexibility. In order to confirm that the peaks in this range are not due to D_2O (which has a peak in the 2200−2700 cm^{-1} range[31]), a spectrum was also measured in H_2O, and the result is shown in Figure S2c. This confirms the presence of peaks at 2850 and 2920 cm^{-1}, along with small shoulder peaks at 2874 and 2960 cm^{-1}.

Next, we measured the CD spectra for 0.5 wt % MALP-2, above the *cac*, for temperatures increasing from 20 to 70 °C, together with the spectrum at 20 °C after cooling from from 70 °C (Figure 2c). The CD spectra in Figure 2c can clearly be assigned to β-sheet structure,[32] as there is a pronounced minimum at 221 nm and a maximum at 200 nm. Similar features in the CD spectra are present for concentrations as low as 0.009 wt % MALP-2 (data not shown). Figure S3 displays the temperature dependence of the molar ellipticity at 221 nm. In good agreement with the FTIR spectra shown in Figure 2a, the CD spectra indicate no significant changes in secondary structure of MALP-2 in solution upon heating. The data in Figure S3 only show a slight reduction in negative molar ellipticity.

The findings from spectroscopic measurements are supported by fiber X-ray diffraction from a dried stalk of MALP-2. The measured fiber X-ray diffraction pattern was found to be isotropic and so were reduced to a radial one-dimensional intensity profile (Figure 3). This shows a sharp peak corresponding to a *d* spacing of 4.66 Å and a series of peaks

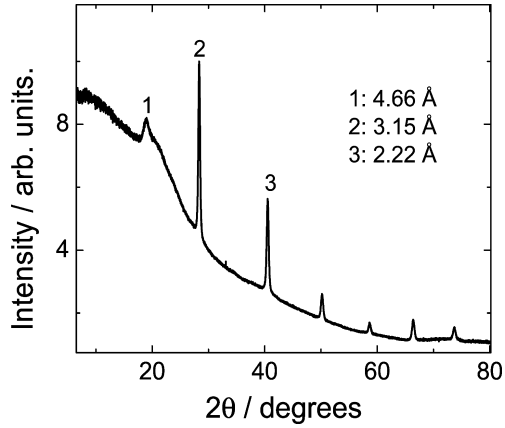

Figure 3. XRD intensity profile obtained from a stalk dried from a 0.5 wt % MALP-2 solution.

with smaller *d*-spacings corresponding to intrapeptide or intralipid chain ordering. The 4.66 Å peak can be assigned to the separation distance of β-strands within β-sheets, as expected for the "cross-β" fiber diffraction pattern from peptides showing β-sheet structure.[33]

Cryo-TEM is a powerful technique to image self-assembled structures via cryo-vitrification of the sample, avoiding potential artifacts associated with drying and/or staining as in conventional negative stain TEM. Cryo-TEM images obtained from solutions of MALP-2 are shown in Figure 4. Remarkable novel "raft-like" structures are observed, which appear to be lateral aggregates of tape-like fibers, extending up to hundreds of nanometers laterally, but with considerable polydispersity in

DOI: 10.1021/acs.biomac.5b01573
Biomacromolecules 2016, 17, 631−640

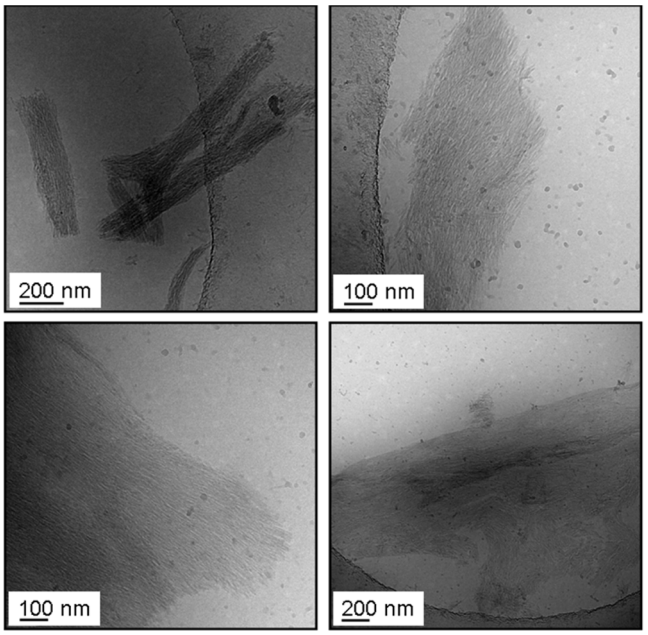

Figure 4. Cryo-TEM images from a 0.5 wt % aqueous solution of MALP-2.

lateral dimensions. The spacing between the fibers in the raft bundles is small, being variable, but always less than 10 nm.

Cryo-TEM was complemented with in situ small-angle X-ray scattering (SAXS), which provides accurate information on the dimensions of the nanostructures and their internal structure. Figure 5 shows intensity profiles measured as a function of temperature for a 0.5 wt % aqueous solution of the lipopeptide, along with model form factor fits. The form factor is that for a lipid bilayer structure, comprising three Gaussian functions to represent the electron density variation across the two headgroups and the dense lipid core.[34] The model and its application to PA bilayer structures have been described in detail in our previous papers.[13b,d] The fitting was implemented using the software SASfit.[35] This form factor provides an excellent fit to the data and confirms that the self-assembled tapes comprise bilayers with a thickness t = 30 Å (at 25 °C) increasing to 35 Å at 60 °C. The other fit parameters are provided in SI, Table S1. The value obtained for the layer thickness t indicates that the bilayers comprise highly interdigitated molecules, with some folded peptide residues and/or disorder in the lipid chain, since the extended length of an hexadecyl PA containing a 13-residue peptide in a parallel β-sheet is expected[36] to be approximately 18 Å (from the C_{16} chain) + 13 × 3.2 Å (from the 13-residue peptide) = 59.6 Å. The SAXS data in Figure 5 shows no major structural transition within the range 20−60 °C, consistent with the FTIR data showing no change in β-sheet structure over this range of temperatures. This points to a high degree of stability of the bilayer structure. We return shortly to present a model for the packing of the MALP-2 molecules.

Self-Assembly of GNNDESNISFKEK. The peptide GNNDESNISFKEK exhibits good solubility in water, with an isoelectric point at pH 4.44 in water, as calculated using Innovagen software.[37] In this work we studied GNNDESNISFKEK concentrations in the range of 0.008−10 wt %. GNNDESNISFKEK solutions exhibited a change in viscosity with increasing concentration, with a sol−gel transition at ∼5

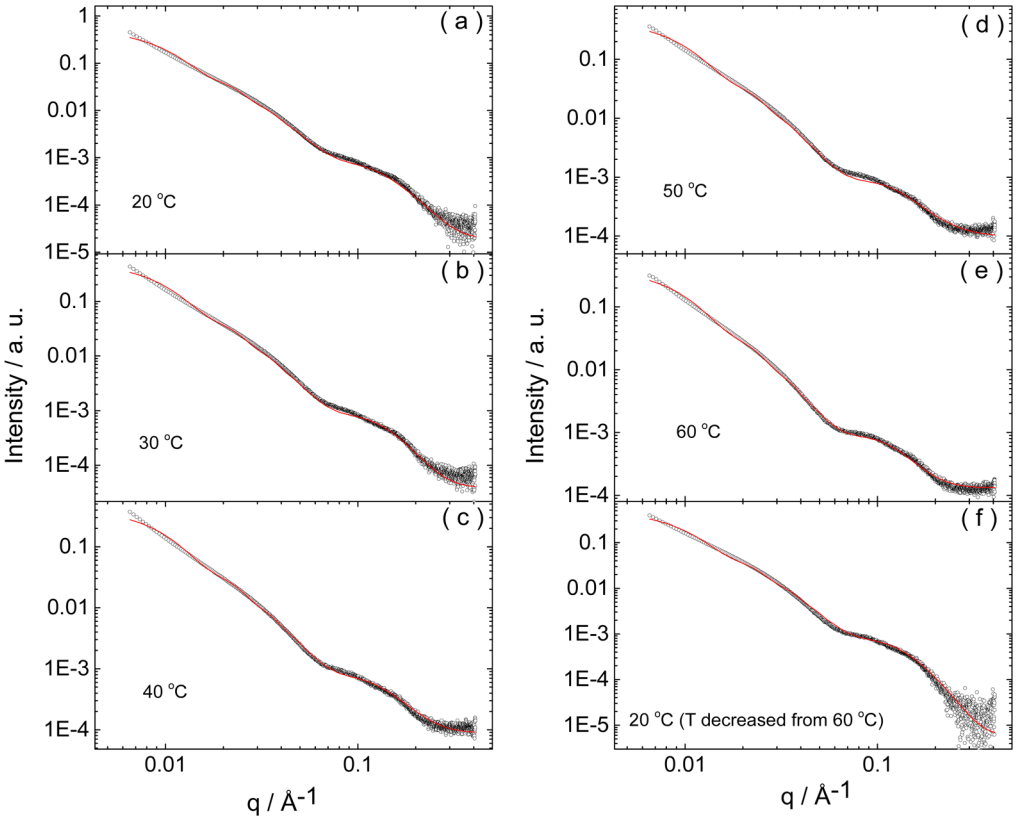

Figure 5. Temperature-dependence of the SAXS intensity profile measured for 0.5 wt % MALP-2 (open symbols) along with bilayer form factor fits (red lines), as described in the text.

DOI: 10.1021/acs.biomac.5b01573
Biomacromolecules 2016, 17, 631−640

wt % peptide, as measured by tube inversion. Figure S4 shows the dependence of the pH on the peptide concentration. The data in Figure S4 together with the dependence of the peptide charge on pH, calculated using the Innovagen software (data not shown),[37] show that the peptide charge slowly increases from ~+1 to ~+3 over the range of concentrations 0.008−10 wt %. Figure S4 also shows the concentration-dependent pH measured for MALP-2.

As mentioned above, ANS is a naphthalene derivative probe that is hardly fluorescent in an aqueous environment but becomes highly fluorescent in apolar environments,[19,22] making it a useful probe to measure the *cac* of peptide solutions. Addition of GNNDESNISFKEK to an aqueous solution of ANS (74 μM) led to a blue shift and an enhancement in the fluorescence emission spectra (inset, Figure 6), supporting the fact that the probe (ANS) moves into a hydrophobic region, which is created by the self-assembly of GNNDESNISFKEK. The *cac* for the peptide is determined as 0.49 wt % from the inflection point of the fluorescence intensity vs concentration plot (Figure 6a). An additional ThT fluorescence assay (Figure 6b) showed that the formation of amyloid fibers takes place at 0.54 wt % peptide, very close to the *cac* determined by ANS. This indicates that hydrophobic collapse and fibril formation occur essentially together, as for the MALP-2 lipopeptide.

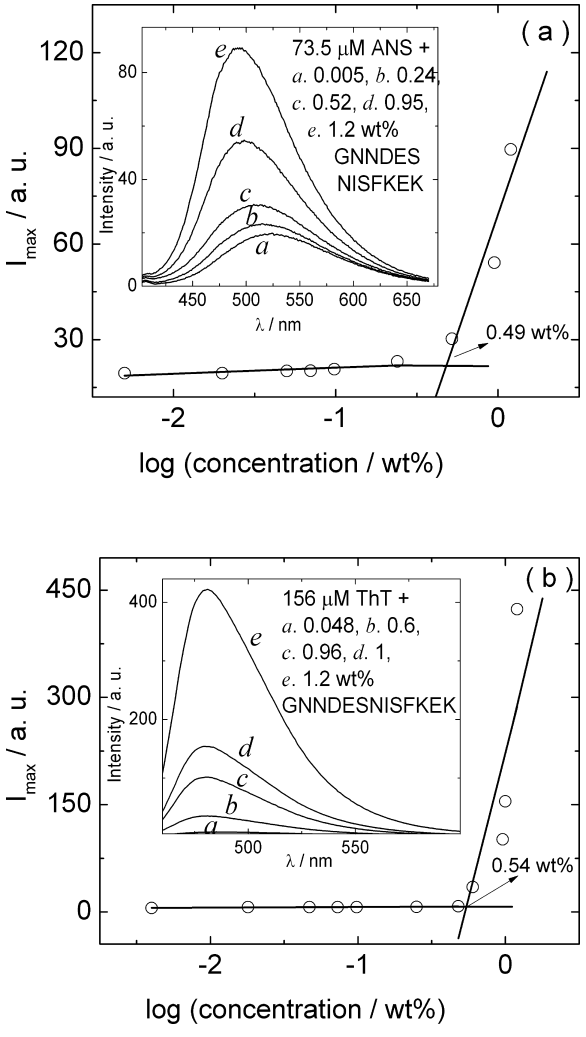

Figure 6. (a) ANS and (b) ThT fluorescence assay to determine the critical aggregation concentration of GNNDESNISFKEK. I_{max} is the intensity at the maximum of the emission curve shown in the inset for some representative concentrations (λ_{ex}= 356 and 440 nm for ANS and ThT respectively).

FTIR spectroscopy was used to investigate secondary structure formation. Spectra covering the amide I′ and amide II′′ regions from 0.5 to 10 wt % peptide are shown in Figure 7a.

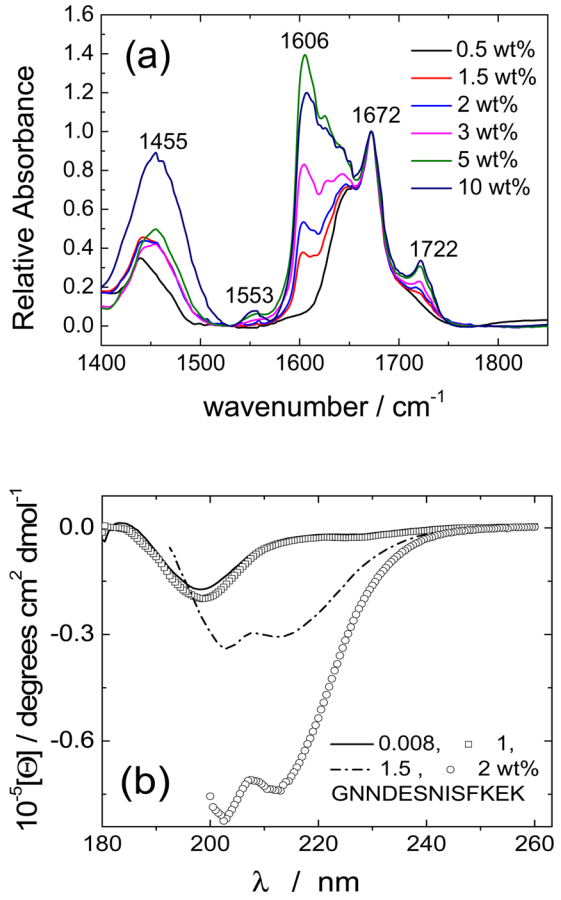

Figure 7. (a) FTIR spectra obtained for 0.5−10 wt % GNNDESNISFKEK (normalized to the peak at 1672 cm^{-1}) and (b) CD spectra obtained for 0.008−2 wt % GNNDESNISFKEK.

All the FTIR spectra exhibit a sharp peak at 1672 cm^{-1} due to bound TFA counterions,[29] which was used to normalize the spectra. Spectra with concentrations between 1.5 and 10 wt % peptide exhibit a peak at 1455 cm^{-1} from side chains[38] and a peak at 1606 cm^{-1} consistent with a frequency-shifted β-sheet peak (reflecting very weak H-bonding).[39] Spectra for samples with concentrations between 3 and 10 wt % peptide exhibit a peak at 1722 cm^{-1} from carboxyl group stretching, while a 1553 cm^{-1} peak (from C═C stretching vibrations[40]) appears for higher concentration samples. The FTIR results in Figure 7a show that there are no major structural changes in the secondary structure upon gel formation. Temperature-dependent FTIR spectra for a sample containing 0.5 wt % peptide (Figure S5), that is, close to the *cac*, show no significant changes with temperature, and this was not examined further for this sample.

CD was used, in addition to FTIR, to assess the secondary structure of GNNDESNISFKEK in solution. The CD spectra measured for 0.008−2 wt % peptide (Figure 7b) are characterized by a deep minimum at 198 nm. Spectra with a negative band centered at about 195−200 nm with no

DOI: 10.1021/acs.biomac.5b01573
Biomacromolecules 2016, 17, 631−640

secondary maximum at about 215−225 nm are characteristic of those of unordered peptide, lacking secondary structure.[41] The CD spectra measured for 2 and 1.5 wt % peptide, characterized by two negative bands at 202 and 213 nm (Figure 7b), are similar to CD spectra assigned to β-turn structures in the literature.[42] The minimum at 213 nm suggests a contribution from β-sheet structure.[32b] While FTIR data does not permit unambiguous assignment of the GNNDESNISFKEK secondary structure, CD shows a clear evolution from a disordered structure below the *cac*, into a structure containing β-sheets (along with β-turns) above the *cac*.

X-ray diffraction patterns measured for stalks prepared using 1 wt % (sol) and 10 (gel) wt % GNNDESNISFKEK showed partial orientation. Therefore, equatorial and meridional sections obtained from 2D XRD images were used to calculate the averaged intensity (Figure 8). The XRD data for 1 wt %

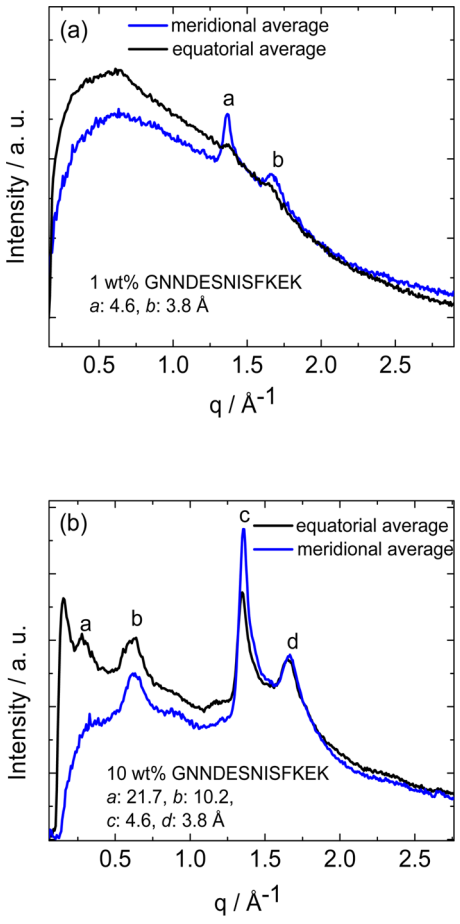

Figure 8. Meridional and equatorial XRD intensity profile obtained from the 2D XRD spectra measured for GNNDESNISFKEK (a) solutions (1 wt % peptide) and (b) gels (10 wt % peptide). The insets display the corresponding 2D spectra.

peptide (Figure 8a) is characterized by reflections at 4.6 and 3.8 Å, corresponding to the β-strand spacing and the spacing between C_α units in the β-sheet, respectively.[33a] A diffuse central scattering peak at 10.5 Å in Figure 8a, can be assigned to the lateral distance between β-sheets.[33a] Similar reflections are present at 4.6, 3.8, and 10.2 Å in the XRD spectra measured for 10 wt % peptide (Figure 8b). In addition, Figure 8b shows a meridional reflection at 21.7 Å, which is close to the "bilayer" width obtained from fitting the SAXS data (Table S2). The expected length of a 13-residue peptide such as GNNDESNISFKEK is 44.2 Å, considering an individual residue spacing of 3.4 Å,[36] so the observed XRD and SAXS data suggest a model with an ordered "core" of β-sheet residues surrounded by more disordered outer hydrophilic residues.

The self-assembled structure formed by GNNDESNISFKEK was examined by cryo-TEM. The images showed the formation of homogeneous twisted tapes 12.3 ± 2.3 nm wide (histogram, Figure S6) and extending to micrometers in length (Figure 9).

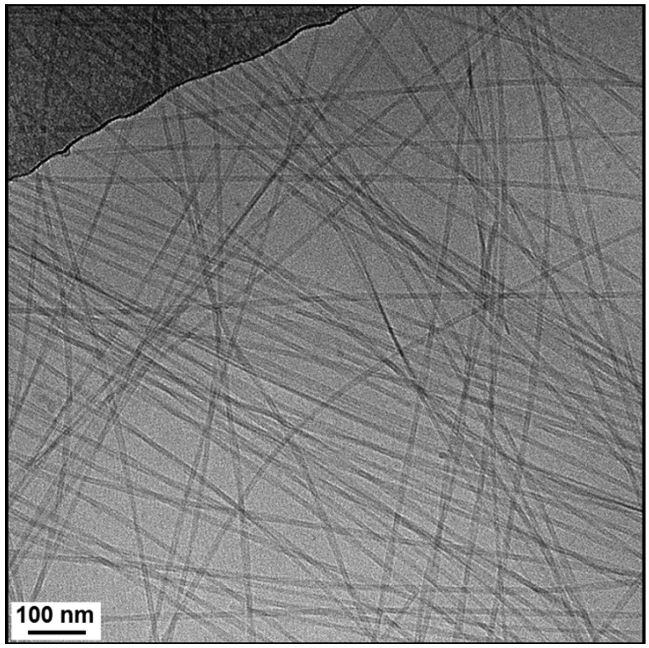

Figure 9. Representative cryo-TEM image from a 2 wt % solution of GNNDESNISFKEK.

The corresponding SAXS profile, along with model form factor fit, is shown in Figure 10. The fit is to a Gaussian bilayer model,

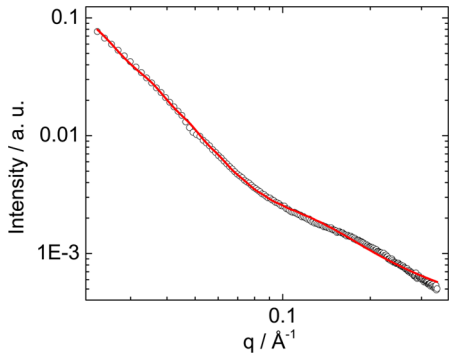

Figure 10. SAXS intensity profile measured for 2 wt % GNNDESNISFKEK (open symbols) along with a bilayer form factor fit (red line), as described in the text.

as for MALP-2. The layer thickness obtained is 18.8 Å, and the other fitting parameters are listed in SI, Table S2. Comparison of the obtained layer thickness to the estimated length of the molecule (and also keeping in mind the value obtained for the lipopeptide) suggests an antiparallel bilayer structure in which the hydrophobic residues are sequestered in the bilayer core while the hydrophilic lysine residues are present at the bilayer surfaces, possibly in a disordered form. A proposed structure is

DOI: 10.1021/acs.biomac.5b01573
Biomacromolecules 2016, 17, 631−640

shown in Figure 11, along with a model for the bilayer structure of MALP-2.

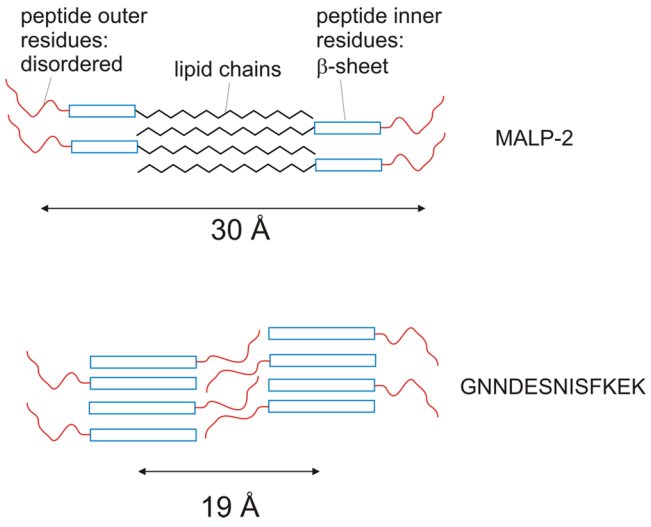

Figure 11. Proposed models for the packing of molecules of MALP-2 and GNNDESNISFKEK.

SUMMARY AND CONCLUSIONS

Through a combination of spectroscopic, scattering, and microscopic methods, we find that MALP-2 self-assembles in water, above a critical aggregation concentration, into unique raft-like bundles of fibers. These are lateral aggregates of short β-sheet fibers. The secondary structure of these fibers is not affected by phase transitions in the lipid chain in the range 25−70 °C. MALP-2 self-assembles into nanotape structures based on bilayers, consistent with amphiphilic nature of the molecule. Since the obtained bilayer thickness is significantly less than that expected for an extended conformation of the chains, we propose a model of fully interdigitated lipid chains, with the attached peptide also largely in a disordered conformation although the inner residues closest to the lipid chains are involved in intermolecular H-bonding interactions as CD, FTIR, and XRD all point to the presence of β-sheet features. In our previous studies on lipopeptide self-assemblies the bilayer thickness is consistent with the all or most of the peptide sequence being incorporated into β-sheet assemblies.[24a,25,43] We suggest that the situation may differ in MALP-2 due to the nature of the ((2-amino-3-oxobutyl)thio)propane-1,2-diyl linker to the two palmitoyl chains, which is different to the direct ester linkage between single palmitoyl chains and the peptide in the lipopeptides previously studied by our group and others. This is probably more important than the length of the peptide sequence, which may also have an influence on secondary structure, since it might be expected that outer residues in a lengthy peptide attached to a lipid chain would tend to adopt a less ordered conformation. Indeed, work by the Hartgerink and Stupp groups shows that in lipopeptides (single palmitoylated peptides) the first few (ca. four) residues closest to the lipid chain are intermolecularly H-bonded, driving β-sheet secondary structures, and indeed it has been shown that *N*-methylation of such residues disrupts this.[44] Outer residues will have greater conformational flexibility and so a higher propensity to adopt less ordered secondary structures. Nonetheless, even for PAs incorporating similar length peptides to that in MALP-2 such as the 13-residue sequence in C_{16}-YEALRVANEVTLN, the measured bilayer spacing (51 Å) suggests an extended peptide conformation with β-sheet ordering extending significantly along the peptide chain, although the total spacing is still less than that for an extended β-strand + lipid chain.[45] For this reason, it is suggested that the nature of the linker in MALP-2 is one key influence on the ordering of the peptide residues, although the presence of multiple lysine residues is also expected to hinder β-sheet formation by the outer residues, due to electrostatic repulsion. Deconvoluting these different influences requires the design of lipopeptides with systematically varied linkers and peptide sequences, which will be an interesting subject for future research.

The constituent peptide within MALP-2, GNNDESNISFKEK, self-assembles in water at a concentration ∼0.5 wt % peptide, much higher than the *cac* for MALP-2, due to the absence of the hydrophobic lipid chain in the chemical structure. GNNDESNISFKEK forms extended twisted tape-like structures. This is in marked contrast to the remarkable raft-like fiber bundles observed for MALP-2. At high concentration, β-sheets of GNNDESNISFKEK are arranged in a proposed antiparallel arrangement. It is evident from our results that, although the lipid chain directs the self-assembly of MALP-2, it also disrupts the fibrillization, generating shorter fibers than those obtained for the peptide alone. In the case of both MALP-2 and its constituent peptide, our SAXS results indicate that a significant fraction of the peptide, presumed to be the outer hydrophilic residues, is in a disordered conformation. In MALP-2, the inner GNNDES··· residues are tethered to the lipid chains in the interior of the bilayer assemblies; however, in the case of the nonlipidated peptide, there is no lipid chain anchor and in this case the GNNDES residues are proposed to lie in the interior of antiparallel layer structures (Figure 11).

Our results highlight the substantial influence of the lipid chain attachment on the peptide to the self-assembled nanostructure. The dipalmitoyl chains, linked to the peptide via a flexible chiral linker in MALP-2 facilitate lateral interactions between the fibers, producing raft-like self-assembled structures. In future work it will be interesting to examine whether this self-assembly motif has any influence on bioactivity, although this can already be observed at very low concentrations (pM−nM,[1,14b] 1 pM = 2.1×10^{-10} wt %), well below the *cac*. The unprecedented raft-like structures are interesting intermediates between planar nanosheet or tape structures and isolated fibrils and suggest that in MALP-2 the balance between the intermolecular interactions that typically favor one or other of these structures is very fine. Strong hydrophobic interactions of lipid chains in lipopeptides typically lead to nanotape structures based on bilayers, whereas strong β-sheet fibrillization favors peptide fibril formation. The peptide fibril raft structure observed for MALP-2 may be an intermediate structure between these two cases. In a previous study,[46] the formation of hexagonally ordered lipopeptide filament bundles (induced by X-ray irradiation) was observed. Bundle formation was ascribed to the growth of new charged filaments constrained by (entropic) forces within the channels of the pre-existing loose filament network, the new filaments interacting through enhanced electrostatic forces between lipopeptides induced by X-ray induced carboxyl group ionization. In our studies, X-ray beam damage was not observed, nevertheless electrostatic effects will be important in interpeptide interactions due to the presence of multiple

DOI: 10.1021/acs.biomac.5b01573
Biomacromolecules 2016, 17, 631−640

charged residues, especially at the C terminus. In the case of MALP-2, the cryo-TEM images have been taken several days after sample preparation which indicates rafts are formed and are stable over such a period, and in addition, temperature-dependent SAXS experiments show (Figure 5) the stability of bilayer nanostructures under thermal cycling across the lipid chain melting temperature. Understanding the kinetics of aggregation and of raft formation are an interesting challenge for future work.

■ ASSOCIATED CONTENT

Supporting Information

The Supporting Information is available free of charge on the ACS Publications website at DOI: 10.1021/acs.biomac.5b01573.

NMR data and peak assignments, SAXS fitting parameters, FTIR spectral deconvolution data, temperature-dependent molar ellipticity figure, concentration-dependent pH data and TEM fiber width histogram (PDF).

■ AUTHOR INFORMATION

Corresponding Author

*E-mail i.w.hamley@reading.ac.uk.

Notes

The authors declare no competing financial interest.

■ ACKNOWLEDGMENTS

This work was supported by an STFC Futures Studentship (ST/L502480/1) that supported the work of S.K. and EPSRC Platform Grant EP/L020599/1. We are grateful to Diamond light source for the award of beamtime on B21 (ref 12321-1) and to Katsuaki Inoue for assistance. We thank Prof. Louis Serpell (Univ. of Sussex) for providing a copy of the program CLEARER. We thank Prof Peter Mühlradt for providing batches of MALP-2 used in initial screening experiments and for helpful discussions. Use of facilities in the Chemical Analysis Facility at the University of Reading is gratefully acknowledged.

■ REFERENCES

(1) Muhlradt, P. F.; Kiess, M.; Meyer, H.; Sussmuth, R.; Jung, G. Isolation, structure elucidation, and synthesis of a macrophage stimulatory lipopeptide from Mycoplasma fermentans acting at picomolar concentration. *J. Exp. Med.* **1997**, *185*, 1951−1958.

(2) Gay, N. J.; Gangloff, M. Structure and function of toll receptors and their Ligands. *Annu. Rev. Biochem.* **2007**, *76*, 141−165.

(3) Mueller, M.; Lindner, B.; Kusumoto, S.; Fukase, K.; Schromm, A. B.; Seydel, U. Aggregates are the biologically active units of endotoxin. *J. Biol. Chem.* **2004**, *279*, 26307−26313.

(4) Shnyra, A.; Hultenby, K.; Lindberg, A. A. Role Of The Physical State Of Salmonella Lipopolysaccharide In Expression Of Biological And Endotoxic Properties. *Infect. Immun.* **1993**, *61* (12), 5351−5360.

(5) (a) Takayama, K.; Din, Z. Z.; Mukerjee, P.; Cooke, P. H.; Kirkland, T. N. Physicochemical Properties of the Lipopolysaccharide Unit that Activates Lymphocytes-B. *J. Biol. Chem.* **1990**, *265*, 14023−14029. (b) Takayama, K.; Mitchell, D. H.; Din, Z. Z.; Mukerjee, P.; Li, C.; Coleman, D. L. Monomeric Re Lipopolysaccharide from Escherichia-Coli is More Active Than the Aggregated Form in the Limulus Amebocyte Lysate Assay and in Inducing Egr-1 Messenger-Rna In Murine Peritoneal-Macrophages. *J. Biol. Chem.* **1994**, *269*, 2241−2244.

(6) Hamley, I. W.; Kirkham, S.; Dehsorkhi, A.; Castelletto, V.; Reza, M.; Ruokolainen, J. Toll-like receptor agonist lipopeptides self-assemble into distinct nanostructures. *Chem. Commun.* **2014**, *50*, 15948−15951.

(7) Barrenschee, M.; Lex, D.; Uhlig, S. Effects of the TLR2 agonists MALP-2 and Pam3Cys in isolated mouse lungs. *PLoS One* **2010**, *5*, e13889.

(8) Shingu, K.; Kruschinski, C.; Luhrmann, A.; Grote, K.; Tschernig, T.; von Horsten, S.; Pabst, R. Intratracheal macrophage-activating lipopeptide-2 reduces metastasis in the rat lung. *Am. J. Respir. Cell Mol. Biol.* **2003**, *28* (3), 316−321.

(9) Deiters, U.; Barsig, J.; Tawil, B.; Muhlradt, P. F. The macrophage-activating lipopeptide-2 accelerates wound healing in diabetic mice. *Exp. Dermatol.* **2004**, *13*, 731−739.

(10) Rharbaoui, F.; Drabner, B.; Borsutzky, S.; Winckler, U.; Morr, M.; Ensoli, B.; Muhlradt, P. F.; Guzman, C. A. The Mycoplasma-derived lipopeptide MALP-2 is a potent mucosal adjuvant. *Eur. J. Immunol.* **2002**, *32*, 2857−2865.

(11) Reppe, K.; Tschernig, T.; Luhrmann, A.; van Laak, V.; Grote, K.; Zemlin, M. V.; Gutbier, B.; Muller, H. C.; Kursar, M.; Schutte, H.; Rosseau, S.; Pabst, R.; Suttorp, N.; Witzenrath, M. Immunostimulation with Macrophage-Activating Lipopeptide-2 Increased Survival in Murine Pneumonia. *Am. J. Respir. Cell Mol. Biol.* **2009**, *40*, 474−481.

(12) (a) Löwik, D. W. P. M.; van Hest, J. C. M. Peptide based amphiphiles. *Chem. Soc. Rev.* **2004**, *33*, 234−245. (b) Matson, J. B.; Zha, R. H.; Stupp, S. I. Peptide self-assembly for crafting functional biological materials. *Curr. Opin. Solid State Mater. Sci.* **2011**, *15*, 225−235. (c) Hamley, I. W. Self-Assembly of Amphiphilic Peptides. *Soft Matter* **2011**, *7*, 4122−4138. (d) Hamley, I. W. Lipopeptides: from self-assembly to bioactivity. *Chem. Commun.* **2015**, *51*, 8574−8583.

(13) (a) Castelletto, V.; Hamley, I. W.; Perez, J.; Abezgauz, L.; Danino, D. Fibrillar superstructure from extended nanotapes formed by a collagen-stimulating peptide. *Chem. Commun.* **2010**, *46*, 9185−9187. (b) Castelletto, V.; Cheng, G.; Stain, C.; Connon, C.; Hamley, I. Self-Assembly of a Peptide Amphiphile Containing L-Carnosine and Its Mixtures with a Multilamellar Vesicle Forming Lipid. *Langmuir* **2012**, *28*, 11599−11608. (c) Jones, R. R.; Castelletto, V.; Connon, C. J.; Hamley, I. W. *Mol. Pharmaceutics* **2013**, *10*, 1063. (d) Castelletto, V.; Gouveia, R.; Connon, C. J.; Hamley, I. W. New RGD-Peptide Amphiphile Mixtures Containing a Negatively Charged Diluent. *Faraday Discuss.* **2013**, *166*, 381−397. (e) Castelletto, V.; Hamley, I. W.; Whitehouse, C.; Matts, P. J.; Osborne, R.; Baker, E. S. Self-assembly of Palmitoyl Lipopeptides Used in Skin Care Products. *Langmuir* **2013**, *29*, 9149−9155. (f) Gouveia, R. M.; Castelletto, V.; Alcock, S. G.; Hamley, I. W.; Connon, C. J. Engineering 3D tissues from 2D peptide amphiphile bioactive films. *J. Mater. Chem. B* **2013**, *1*, 6157−6169.

(14) (a) Takeuchi, O.; Kawai, T.; Muhlradt, P. F.; Morr, M.; Radolf, J. D.; Zychlinsky, A.; Takeda, K.; Akira, S. Discrimination of bacterial lipoproteins by Toll-like receptor 6. *Int. Immunol.* **2001**, *13*, 933−940. (b) Morr, M.; Takechi, O.; Akira, S.; Simon, M. M.; Mühlradt, P. F. Differential recognition of structural details of bacterial lipopeptides by toll-like receptors. *Eur. J. Immunol.* **2002**, *32*, 3337−3347. (c) Hoebe, K.; Georgel, P.; Rutschmann, S.; Du, X.; Mudd, S.; Crozat, K.; Sovath, S.; Shamel, L.; Hartung, T.; Zahringer, U.; Beutler, B. CD36 is a sensor of diacylglycerides. *Nature* **2005**, *433*, 523−527.

(15) Akira, S.; Uematsu, S.; Takeuchi, O. Pathogen recognition and innate immunity. *Cell* **2006**, *124*, 783−801.

(16) Morr, M.; Takeuchi, O.; Akira, S.; Simon, M. M.; Muhlradt, P. F. Differential recognition of structural details of bacterial lipopeptides by toll-like receptors. *Eur. J. Immunol.* **2002**, *32*, 3337−3347.

(17) Muhlradt, P. F.; Kiess, M.; Meyer, H.; Sussmuth, R.; Jung, G. Isolation, structure elucidation, and synthesis of a macrophage stimulatory lipopeptide from Mycoplasma fermentans acting at picomolar concentration. *J. Exp. Med.* **1997**, *185*, 1951−1958.

(18) (a) Wiesmüller, K. H.; Bessler, W.; Jung, G. Synthesis Of The Mitogenic S- 2,3-Bis(Palmitoyloxy)Propyl-N-Palmitoylpentapeptide From Escherichia-Coli Lipoprotein. *Hoppe-Seyler's Z. Physiol. Chem.* **1983**, *364*, 593−606. (b) Metzger, J. W.; Wiesmuller, K. H.; Jung, G. Synthesis of N-Alpha-Fmoc Protected Derivatives of S-(2,3-Dihydrox-

DOI: 10.1021/acs.biomac.5b01573
Biomacromolecules 2016, 17, 631−640

ypropyl)-Cysteine and their Application in Peptide-Synthesis. *Int. J. Pept. Protein Res.* **1991**, *38*, 545−554.
(19) Hawe, A.; Sutter, M.; Jiskoot, W. Extrinsic fluorescent dyes as tools for protein characterization. *Pharm. Res.* **2008**, *25*, 1487−1499.
(20) (a) LeVine, H. Thiflavine-T interaction with synthetic Alzheimers-disease beta-amyloid peptides- detection of amyloid aggregation in solution. *Protein Sci.* **1993**, *2*, 404−410. (b) LeVine, H. Quantification of β-sheet Amyloid Fibril Structures with Thioflavin T. In *Methods in Enzymology*; Wetzel, R., Ed.; Academic Press: San Diego, 1999; Vol. *309*, pp 274−284.
(21) Makin, O. S.; Sikorski, P.; Serpell, L. C. CLEARER: a new tool for the analysis of X-ray fibre diffraction patterns and diffraction simulation from atomic structural models. *J. Appl. Crystallogr.* **2007**, *40*, 966−972.
(22) (a) Lindgren, M.; Sorgjerd, K.; Hammarstrom, P. Detection and Characterization of Aggregates, Prefibrillar Amyloidogenic Oligomers, and Protofibrils Using Fluorescence Spectroscopy. *Biophys. J.* **2005**, *88*, 4200−4212. (b) Gasymov, O. K.; Glasgow, B. J. ANS Fluorescence: Potential to Augment the Identification of the External Binding Sites of Proteins. *Biochim. Biophys. Acta, Proteins Proteomics* **2007**, *1774*, 403−411.
(23) Khurana, R.; Coleman, C.; Ionescu-Zanetti, C.; Carter, S. A.; Krishna, V.; Grover, R. K.; Roy, R.; Singh, S. Mechanism of thioflavin T binding to amyloid fibrils. *J. Struct. Biol.* **2005**, *151*, 229−238.
(24) (a) Castelletto, V.; Gouveia, R. J.; Connon, C. J.; Hamley, I. W. New RGD- Peptide Amphiphile mixtures Containing a Negatively Charged Diluent. *Faraday Discuss.* **2013**, *166*, 381−397. (b) Guler, M. O.; Claussen, R. C.; Stupp, S. I. Encapsulation of pyrene within self-assembled peptide amphiphile nanofibers. *J. Mater. Chem.* **2005**, *15*, 4507−4512. (c) Sabate, R.; Estelrich, J. Evidence of the existence of micelles in the fibrillogenesis of beta-amyloid peptide. *J. Phys. Chem. B* **2005**, *109*, 11027−11032. (d) Fowler, M.; Siddique, B.; Duhamel, J. Effect of Sequence on the Ionization Behavior of a Series of Amphiphilic Polypeptides. *Langmuir* **2013**, *29*, 4451−4459.
(25) Hamley, I. W.; Dehsorkhi, A.; Castelletto, V. Coassembly in Binary Mixtures of Peptide Amphiphiles Containing Oppositely Charged Residues. *Langmuir* **2013**, *29*, 5050−5059.
(26) Hamley, I. W.; Kirkham, S.; Dehsorkhi, A.; Castelletto, V.; Adamcik, J.; Mezzenga, R.; Ruokolainen, J.; Mazzuca, C.; Gatto, E.; Venanzi, M.; Placidi, E.; Bilalis, P.; Iatrou, H. Self-Assembly of a Model Peptide Incorporating a Hexa-Histidine Sequence Attached to an Oligo-Alanine Sequence, and Binding to Gold NTA/Nickel Nanoparticles. *Biomacromolecules* **2014**, *15*, 3412−3420.
(27) (a) Cameron, D. G.; Casal, H. L.; Mantsch, H. H. Characterization of the pretransition in 1,2-dipalmitoyl-sn-glycero-3-phosphocholine by Fourier-transform infrared spectroscopy. *Biochemistry* **1980**, *19*, 3665−3672. (b) Casal, H. L.; Mantsch, H. H. Polymorphic phase-behaviour of phospholipid-membranes studied by infrared spectroscopy. *Biochim. Biophys. Acta, Rev. Biomembr.* **1984**, *779*, 381−401.
(28) (a) Jackson, M.; Mantsch, H. H. The use and misuse of FTIR spectroscopy in the determination of protein-structure. *Crit. Rev. Biochem. Mol. Biol.* **1995**, *30*, 95−120. (b) Stuart, B. *Biological Applications of Infrared Spectroscopy*; Wiley: Chichester, 1997.
(29) (a) Pelton, J. T.; McLean, K. R. Spectroscopic methods for analysis of protein secondary structure. *Anal. Biochem.* **2000**, *277*, 167−176. (b) Gaussier, H.; Morency, H.; Lavoie, M. C.; Subirade, M. Replacement of trifluoroacetic acid with HCl in the hydrophobic purification steps of pediocin PA-1: A structural effect. *Appl. Environ. Microbiol.* **2002**, *68*, 4803−4808. (c) Eker, F.; Griebenow, K.; Schweitzer-Stenner, R. A beta(1−28) fragment of the amyloid peptide predominantly adopts a polyproline II conformation in an acidic solution. *Biochemistry* **2004**, *43*, 6893−6898.
(30) Cameron, D. G.; Casal, H. L.; Mantsch, H. H. The Application of Fourier Transform Infrared Transmission Spectroscopy to the Study of Model and Natural Membranes. *J. Biochem. Biophys. Methods* **1975**, *1*, 21−36.
(31) Maréchal, Y. Infrared spectra of water. I. Effect of temperature and of H/D isotopic substitution. *J. Chem. Phys.* **1991**, *95*, 5565−5573.
(32) (a) Sreerama, N.; Woody, R., Circular Dichroism of Peptides and Proteins. In *Circular Dichroism: Principles and Applications*, 2nd ed.; Berova, N., Nakanishi, K., Woody, R. W., Eds.; John Wiley: New York, 2000. (b) Kelly, S. M.; Jess, T. J.; Price, N. C. How to study proteins by circular dichroism. *Biochim. Biophys. Acta, Proteins Proteomics* **2005**, *1751*, 119−139. (c) Hamley, I. W. Peptide fibrillization. *Angew. Chem., Int. Ed.* **2007**, *46*, 8128−8147. (d) Nordén, B.; Rodger, A.; Dafforn, T. R. *Linear Dichroism and Circular Dichroism: A Textbook on Polarized-light Spectroscopy*; RSC Publishing: Cambridge, 2010.
(33) (a) Serpell, L. C. Alzheimer's amyloid fibrils: structure and assembly. *Biochim. Biophys. Acta, Mol. Basis Dis.* **2000**, *1502*, 16−30. (b) Gras, S. L. Amyloid fibrils: From disease to design. New biomaterial applications for self-assembling cross-beta fibrils. *Aust. J. Chem.* **2007**, *60*, 333−342.
(34) Pabst, G.; Rappolt, M.; Amenitsch, H.; Laggner, P. Structural Information from Multilamellar Liposomes at Full Hydration: Full q-Range Fitting with High Quality X-Ray Data. *Phys. Rev. E: Stat. Phys., Plasmas, Fluids, Relat. Interdiscip. Top.* **2000**, *62*, 4000−4008.
(35) Bressler, I.; Kohlbrecher, J.; Thünemann, A. F. SASfit: a tool for small-angle scattering data analysis using a library of analytical expressions. *J. Appl. Crystallogr.* **2015**, *48*, 1587−1598.
(36) Creighton, T. E. *Protein Folding*; W.H. Freeman: New York, 1992.
(37) Innovagen's Peptide Property Calculator. Innovagen AB, 2015; www.innovagen.se/custom-peptide-synthesis/peptide-property-calculator/peptide-property-calculator.asp.
(38) (a) Marin-Argany, M.; Candel, A. M.; Murciano-Calles, J.; Martinez, J. C.; Villegas, S. The interconversion between a flexible β-sheet and a fibril β-arrangement constitutes the main conformational event during misfolding of PSD95-PDZ3 domain. *Biophys. J.* **2012**, *103*, 738−747. (b) Arrondo, J. L.; Muga, A.; Castresana, J.; Goni, F. M. Quantitative studies of the structure of proteins in solution by Fourier-transform infrared spectroscopy. *Prog. Biophys. Mol. Biol.* **1993**, *59*, 23−56.
(39) Castelletto, V.; Hamley, I. W.; Adamcik, J.; Mezzenga, R.; Gummel, J. Modulating self-assembly of a nanotape-forming peptide amphiphile with an oppositely charged surfactant. *Soft Matter* **2012**, *8*, 217−226.
(40) Bellamy, L. J. *The infra-red spectra of complex molecules*. Chapman and Hall: London, 1975.
(41) (a) Toniolo, C.; Formaggio, F.; Woody, R. W. In *Electronic Circular Dichroism of Peptides*; Berova, N., Polavarapu, P. L., Nakanishi, K., Woody, R. W., Eds.; Wiley: New York, 2012. (b) Paramonov, S. E.; Jun, H. W.; Hartgerink, J. D. Self-assembly of peptide-amphiphile nanofibers: The roles of hydrogen bonding and amphiphilic packing. *J. Am. Chem. Soc.* **2006**, *128*, 7291−7298.
(42) Perczel, A.; Hollosi, M.; Foxman, B. M.; Fasman, G. D. Conformational Amalysis of Pseudocyclic Hexapeptides Based on Quantitative Circular Dichroism (CD), NOE, and X-ray Data. The pure CD Spectra of Type I and Type II β-turns. *J. Am. Chem. Soc.* **1991**, *113*, 9772−9784.
(43) Castelletto, V.; Hamley, I. W.; Perez, J.; Abezgauz, L.; Danino, D. Fibrillar superstructure from extended nanotapes formed by a collagen-stimulating peptide. *Chem. Commun.* **2010**, *46*, 9185−9187.
(44) (a) Paramonov, S. E.; Jun, H.-W.; Hartgerink, J. D. Self-assembly of peptide-amphiphile nanofibers: The roles of hydrogen bonding and amphiphilic packing. *J. Am. Chem. Soc.* **2006**, *128*, 7291−7298. (b) Ortony, J. H.; Newcomb, C. J.; Matson, J. B.; Palmer, L. C.; Doan, P. E.; Hoffman, B. M.; Stupp, S. I. Internal dynamics of a supramolecular nanofibre. *Nat. Mater.* **2014**, *13*, 812−816.
(45) Hamley, I. W.; Dehsorkhi, A.; Castelletto, V.; Walter, M. N. M.; Connon, C. J.; Reza, M.; Ruokolainen, J. Self-Assembly and Collagen Stimulating Activity of a Peptide Amphiphile Incorporating a Peptide Sequence from Lumican. *Langmuir* **2015**, *31*, 4490−4495.
(46) Cui, H. G.; Pashuck, E. T.; Velichko, Y. S.; Weigand, S. J.; Cheetham, A. G.; Newcomb, C. J.; Stupp, S. I. Spontaneous and X-ray-Triggered Crystallization at Long Range in Self-Assembling Filament Networks. *Science* **2010**, *327*, 555−559.

DOI: 10.1021/acs.biomac.5b01573
Biomacromolecules 2016, 17, 631−640